# Estimation of $CH_4$ emission based on advanced 4D-LETKF assimilation system

Jagat S. H. Bisht[1]*, Prabir K. Patra[1,2], Masayuki Takigawa[1], Takashi Sekiya[1], Yugo Kanaya[1], Naoko Saitoh[2], and Kazuyuki Miyazaki[3]

[1]Research Institute for Global Change, JAMSTEC, Yokohama, 235-0019, Japan

[2]Center for Environmental Remote Sensing, Chiba University, Chiba, 263-8522, Japan

[3]Jet Propulsion Laboratory/California Institute for Technology, Pasadena, CA, USA,

*corresponding author's e-mail: jagatbisht@jamstec.go.jp

## Abstract

Methane ($CH_4$) is the second major greenhouse gas after carbon dioxide ($CO_2$) which has substantially increased during last decades in the atmosphere, raising serious sustainability and climate change issues. Here, we develop a data assimilation system for in situ and column averaged concentrations using Local ensemble transform Kalman filter (LETKF) to estimate surface emissions of $CH_4$. The data assimilation performance is tested and optimized based on idealized settings using Observation System Simulation Experiments (OSSEs) where a known surface emission distribution (the truth) is retrieved from synthetic observations. We tested three covariance inflation methods to avoid covariance underestimation in the emission estimates, namely; fixed multiplicative (FM), relaxation to prior spread (RTPS) and adaptive multiplicative. First, we assimilate the synthetic observations at every grid point at the surface level. In such a case of dense observational data, the normalized Root Mean Square Error (RMSE) in the analyses over global land regions are smaller by 10-15% in case of RTPS covariance inflation method compared to FM. We have shown that integrated estimated flux seasonal cycles over 15 regions using RTPS inflation are in reasonable agreement between true and estimated flux with 0.04 global normalized annual mean bias. We have then assimilated the column averaged $CH_4$ concentration by sampling the model simulations at GOSAT observation locations and time for another OSSE experiment. Similar to the case of dense observational data, RTPS covariance inflation method performs better than FM for GOSAT synthetic observation in terms of normalized RMSE (2-3%) and integrated flux estimation comparison with the true flux. The annual mean averaged normalized RMSE (normalized mean bias) in LETKF $CH_4$ flux estimation in case of RTPS and FM covariance inflation is found to be 0.59 (0.18) and 0.61 (0.23) respectively. The chi-square test performed for GOSAT synthetic observations assimilation suggests high underestimation of background error covariance in both RTPS and FM covariance inflation

methods, however, the underestimation is much higher (>100% always) for FM compared to RTPS covariance inflation method.

## 1. Introduction

Methane ($CH_4$) is the second major greenhouse gas, after carbon dioxide ($CO_2$), that has anthropogenic sources. According to the contemporary record of the global $CH_4$ budget, the total of all $CH_4$ sources ranges 538–593 Tg $yr^{-1}$ during 2008–2017 (Saunois et al., 2020). The primary natural sources are from wetlands (~40%). The main anthropogenic $CH_4$ emissions are from microbial emissions associated with ruminant (livestock and waste), rice cultivation, fugitive emissions (oil and gas production and use), and incomplete combustion of bio and fossil fuels. The major fraction of atmospheric $CH_4$ sinks (range: 474 - 532 Tg $yr^{-1}$) occurs in the troposphere by oxidation via reaction with hydroxyl (OH) radicals (Patra, et al., 2011; Saunois et al., 2020); other loss processes include oxidation by soil, and reactions with $O^1D$ and Cl. The lifetime of $CH_4$ in the atmosphere is estimated to be 9.1 ± 0.9 years (Szopa et al. 2021).

Regional $CH_4$ emissions can be estimated from $CH_4$ concentration fields and chemistry transport models using Bayesian synthesis approaches based on inverse modeling techniques (e.g., Enting, 2002). In such approach, emissions are optimized on a coarse resolution (e.g., for a limited number of pre-defined regions) mostly using surface-based observations. $CH_4$ concentrations are provided by the NOAA cooperative air sampling network sites (Dlugokencky et al., 2020) and other networks by the World Data Centre for Greenhouse Gases (WDCGG) website, hosted by the Japan Meteorological Agency. In the recent years, satellite measurements are made from the Greenhouse Gases Observing Satellite (GOSAT) or the TROPOspheric Monitoring Instrument (TROPOMI) (Lorente et al., 2021), covering the globe with fine spatio-temporal scales. GOSAT provide an extensive global observations of column $CH_4$ concentrations since 2009 (Yoshida et al., 2013). Some of the inverse modeling studies utilize the satellite observations for $CH_4$ flux estimation (Zhang et al., 2021; Maasakkers et al., 2016), but, it requires enormous computational resources while dealing with more flux regions and more observations.

Grid-based $CH_4$ flux optimization is also performed using adjoint technique (4-D Var data assimilation) and Ensemble Kalman Filter (EnKF), but was limited to small sets of observations (Houweling et al., 1999; Meirink et al., 2008; Bruhwiler et al., 2014). Bruhwiler et al. (2014) followed the EnKF method of Peters et al. (2005) to estimate the $CH_4$ surface fluxes that utilizes an off-line ACTM framework. Techniques such as 4-D Var and EnKF are important to estimate $CH_4$ fluxes since they can assimilate a large number of observations, manage high-resolution fluxes. In the EnKF system, a flow-dependent forecast error covariance structure is provided by ensemble model forecasts, while it does not need an adjoint model that makes it simple but powerful tool for flux estimation.

One of the limitations in EnKF method is the dependence of the resolution of state vector on ensemble size, which can give spurious results if the number of ensemble members is much smaller than the rank of the error covariance matrix (Houtekamer and Zhang, 2016).

LETKF is a type of square-root EnKF that performs analysis locally in space without perturbing the observations (Ott et al., 2002, 2004; Hunt et al., 2007). LETKF is computationally efficient since the observations are assimilated simultaneously not serially, it is simple to account for observation error correlation. Miyazaki et al. (2011) and Kang et al. (2012) demonstrated the implementation of LETKF data assimilation system by coupling an ACTM for carbon-cycle research using atmospheric $CO_2$ observations. It is also extensively applied for the emission estimation of short-lived species using satellite data (Skachko et al., 2016; Miyazaki et al., 2019; Sekiya et al., 2021). In this work, we will estimate the $CH_4$ fluxes using a LETKF data assimilation system. Assimilation windows ranging from 6 hours (Kang et al., 2012) to several months (Bruhwiler et al., 2014) have been used, depending on the desired time resolution of the estimated emissions, which is often limited by the observational data density. The time frame over which the system behaves linearly, and in what time frame the observations respond to the control variables such as, atmospheric transport, as well as observation abundance, must also be taken into consideration. Within an assimilation window, where and when the fluxes would be constrained by specific observations is to be ascertained by the correlation between ensemble prior fluxes and the ensemble $CH_4$ concentrations simulation from a forward model (Liu et al., 2016).

Main objective of this work is to develop an advanced 4-D data assimilation system based on LETKF that simultaneously estimates atmospheric distributions and surface fluxes of $CH_4$. OSSEs are conducted to assess the performance of LETKF since it is important to test the system against the known emissions or the truth. The OSSE LETKF set-up of top-down $CH_4$ flux estimation using online ACTM is an essential step before implementing on real in situ and satellite observation.

## 2. Formulation of LETKF system

We briefly describe the LETKF in the application of $CH_4$ flux estimation, while detailed derivation of equations and code implementation are given elsewhere (Hunt et al., 2007; Miyazaki et al., 2011; Miyoshi et al., 2010). The notation used here for LETKF formulation is adopted from Kotsuki et al. (2017). In the LETKF, the background ensemble (columns of matrix $x^b$) in a local region evolved from a set of perturbed initial conditions. The background ensemble mean, $\bar{x}^b$, and its perturbation, $X^b$, are estimated from the ensemble forecast such as:

$$\bar{x}^b = \frac{1}{m}\sum_{i=1}^{m} x_i^b ; \quad X_i^b = x_i^b - \bar{x}^b \qquad (1)$$

Where 'm' indicates the ensemble size. The background error covariance matrix $P^b$ in the m-dimensional ensemble is defined as:

$$P^b = \frac{1}{m-1} X^b \left[X^b\right]^T \quad (2)$$

The analysis ensemble mean $\bar{x}^a$ is derived using background ensemble mean $\bar{x}^b$ and ensemble perturbations $X^b$ such as:

$$\bar{x}^a = \bar{x}^b + X^b \tilde{P}^a \left(Y^b\right)^T R^{-1} \left(y^o - H\bar{x}^b\right) = \bar{x}^b + X^b w^a \quad (3)$$

where H, Y, R, and $\tilde{P}^a$ denote the linear observation operator, ensemble perturbation matrix in the observation space ($Y \equiv Hx$), observation error covariance matrix, and analysis error covariance matrix in the ensemble space, respectively. The superscripts 'o', 'b' and 'a' denote the observations, background (prior), and analysis (posterior), respectively. $w^a$ defines the analysis increment (or analysis weight) in observation space and is derived using the information about observational increment $y^o - H\bar{x}^b$. The analysis error covariance matrix ($\tilde{P}^a$) in the m-dimensional ensemble space is spanned by ensemble perturbation (Hunt et al., 2007) and defined as:

$$\tilde{P}^a = \{(m-1)I + \left(HX^b\right)^T R^{-1} HX^b\}^{-1} \quad (4)$$

Finally, the analysis ensemble perturbations $X^a$ at the central grid point are derived such as:

$$X^a = X^b \{(m-1)\tilde{P}^a\}^{1/2} \quad (5)$$

Where, $\{(m-1)\tilde{P}^a\}^{1/2}$ is a multiple of the symmetric square root of the local analysis error covariance matrix in ensemble space and could be computed by singular vector decomposition method.

We have applied a gross error check as a quality control to exclude observations that are far from the first guess, the appropriate degrees of the gross error check are also examined. Figure 1 shows the schematic diagram of our LETKF set-up with two ensemble members for 3 consecutive assimilation cycles with 8 days assimilation window. The analysis is obtained at mid-point time of the assimilation window (Figure 1). The analyzed (updated) surface flux is used for next data assimilation cycle starting from the mid-point time of the previous data assimilation window. The state vector augmentation approach is used to estimate the atmospheric $CH_4$ surface flux (Kang et al., 2012; Miyazaki et al., 2011).

Assimilation window size and ensemble members are chosen based on computational efficiency and estimation accuracy. A larger assimilation window means fluxes are constrained by more

observations, however, it requires handling of large matrix optimization which is difficult in cases of dense observation and introduces sampling errors related to transport errors. In this study, few sensitivity experiments performed to demonstrate the choice of assimilation window length and ensemble size when GOSAT synthetic observation are assimilated in Section 4.2.

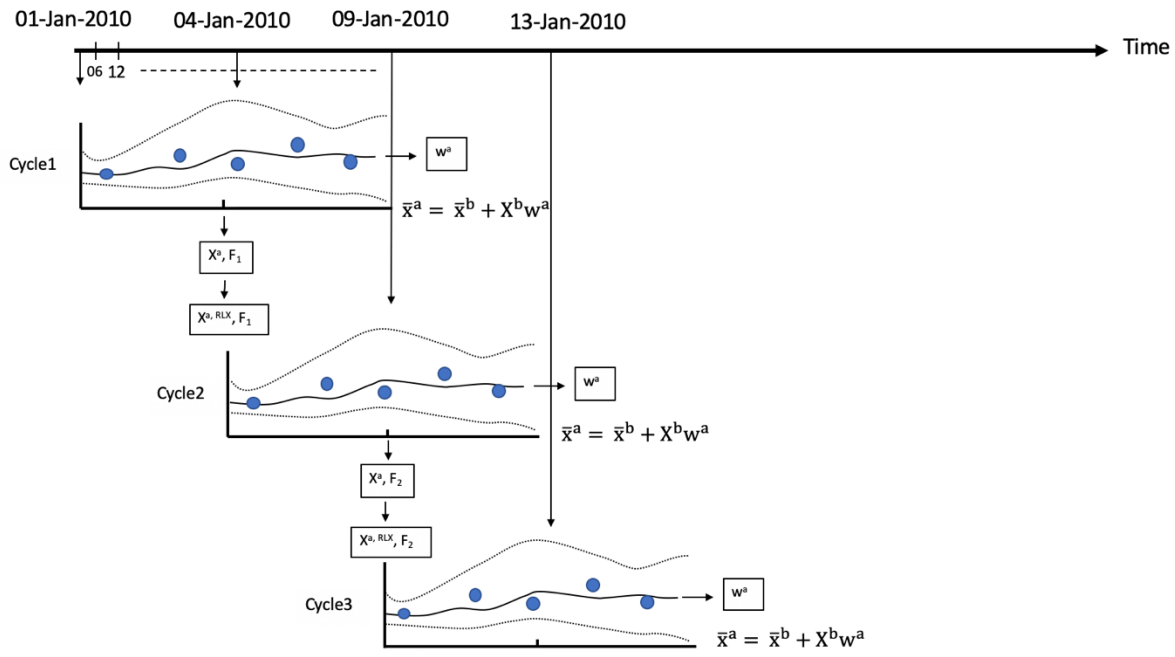


**Figure 1:** Schematic represents the temporal evolution of LETKF cycle. In the first assimilation window (Cycle1), the dotted lines show the ensemble forecast of $CH_4$ concentrations (with 2 ensemble members), the solid line shows the linear combination of the forecasts, the filled circles show the observations of $CH_4$ concentration. The data assimilation finds the linear combination of the ensemble forecast by estimating the weight ($w^a$) that best fits the observations throughout the assimilation window. The analysis weight is applied to obtain optimal surface fluxes (F) and the concentration of $CH_4$ at the intermediate time of the data assimilation window. The updated analyzed concentration ensembles are used as initial condition after relaxation ($X^{a,RLX}$) (Eq. 8) for the next ensemble forecast. The spread of the ensemble members represents the forecast error. The schematic is adapted from Kalnay & Yang (2010) and Miyazaki et al. (2011).

### 2.1 Covariance inflation

The LETKF data assimilation needs variance inflation to mitigate the under dispersive ensemble. We tested three methods; fixed multiplicative (FM), relaxation-to-prior spread (RTPS), and adaptive multiplicative covariance inflation.

The fixed multiplicative (FM) inflation method (Anderson and Anderson, 1999) inflates the prior ensemble by inflating the background error covariance matrix $P^b$ defined in equation (Eq. 2) such as:

$$P^{b}_{inf} = \gamma P^{b}_{tmp} \quad (6)$$

where $P^{b}_{tmp}$ represents the temporary background error covariance matrix which is inflated by a factor $\gamma$.

The other inflation methods used to prevent the reduction of ensemble spread are relaxation-to-prior perturbation (RTPP) (Zhang et al., 2004) and relaxation-to-prior spread (RTPS) (Whitaker and Hamill, 2012). The RTPP methods relax the reduction of the ensemble spread after updating the ensemble perturbations which blends the background and analysis ensemble perturbations as:

$$X^{a}_{inf} = \alpha_{RTPP} X^{b} + (1 - \alpha_{RTPP}) X^{a}_{tmp} \quad (7)$$

where $\alpha_{RTPP}$ denotes the relaxation parameter of the RTPP.

The RTPS inflation method relaxes the reduction of ensemble spread by relaxing the analysis spread to prior spread such as:

$$X^{a}_{RLX} = \left( \frac{\alpha_{RTPS}\sigma^{b} + (1 - \alpha_{RTPS})\sigma^{a}}{\sigma^{a}} \right) X^{a}_{tmp} \quad (8)$$

where $\sigma$ and $\alpha_{RTPS}$ denote the ensemble spread, and relaxation parameter of the RTPS, respectively. The range of parameter $\alpha_{RTPS}$ is bounded by [0, 1]. This study focuses mainly on the FM and RTPS covariance inflation methods.

In addition, Miyoshi (2011) applied adaptive inflation by determining the multiplicative inflation factors at every grid point at every analysis step using the observation-space statistics derived by Daley (1992) and Desroziers et al. (2005).

$$< dd^{T} > = HP^{b}_{inf}H^{T} + R \quad (9)$$

Where the operator '<•>' denotes the statistical expectation and $d = y^{o} - H\bar{x}^{b}$ (observation-minus-first-guess), and R is the error observation covariance matrix.

The impact of using the adaptive multiplication inflation method is discussed in the GOSAT synthetic observation assimilation experiments in Section 4.2.

## 2.2 MIROC4-ACTM

Model for Interdisciplinary Research on Climate, version 4.0 (MIROC4) based ACTM (hereafter referred to as MIROC4-ACTM) (Patra et al., 2018; Bisht et al., 2021) is used here for $CH_4$ concentration simulations. The model simulations have been performed at horizontal grid resolution of approximately 2.8×2.8° latitude-longitude grid (T42 spectral truncations) and hybrid vertical

coordinate of 67 levels (Earth's surface to 0.0128 hPa, Watanabe et al., 2008). Bisht et al., 2021 performed the multi-tracer analysis and demonstrated the importance of very well-resolved stratosphere in the MIROC4-ACTM that illustrates better extratropical stratospheric variabilities, and simulated tropospheric dynamical fields. The meteorological fields in MIROC4-ACTM are nudged to the JMA Re-analysis (JRA-55) data (Kobayashi et al., 2015).

## 3. Experimental set-up

### 3.1 Construction of known surface emissions (truth)

Present OSSEs intend to develop basic tuning strategies before the actual data to be assimilated which is useful to accelerate the operational use of real observations. The OSSE has been discussed here by exploiting the known "truth". The synthetic observations to be assimilated in the OSSE are generated from nature runs which uses bottom-up surface emission (true) data to simulate global 3-D $CH_4$ concentrations. The true surface $CH_4$ emissions are prepared on the monthly scale using anthropogenic and natural sectors, minus the surface sinks due to bacterial consumption in the soil (Chandra et al., 2021). The anthropogenic emissions were obtained from the Emission Database for Global Atmospheric Research, version 4.3.2 inventory (EDGARv4.3.2) (Maenhout et al., 2019) that includes the emissions from the major sectors such as; fugitive, enteric fermentation and manure management, solid waste and wastewater handling. The biomass burning emissions are taken from the Global Fire Database (GFEDv4s) (van der Werf et al., 2017) and Goddard Institute for Space Studies emissions (Fung et al., 1991). The wetland and rice emissions are taken from the process-based model of the terrestrial biogeochemical cycle, Vegetation Integrated Simulator of Trace gases (VISIT) (Ito, 2019) that is based on Cao et al. (1996). The other natural emission such as, ocean, termites, mud volcano are taken from TransCom-$CH_4$ inter-comparison experiment (Patra et al., 2011). The total emissions are taken as the truth for the OSSEs and the concentration simulated by MIROC4-ACTM will be referred to as synthetic observations.

### 3.2 Prior flux preparation and LETKF setting

Based on our understanding of $CH_4$ inverse modelling, the uncertainty in regional flux estimation is found to be 30% or lower (Chandra et al., 2021). Therefore, we attempted to reproduce the true flux by starting with a prior flux that is lower by 30% of the true flux (prior flux has same seasonal cycles as true flux). The MIROC4-ACTM is initialized with the spin-up of 3 years (2007 – 2009) with prior flux distribution. The initial $CH_4$ distribution on 01 January 2007 was taken from an earlier simulation of 27 years. An initial perturbation with standard deviation of approximately 6-8% spread is applied to the a priori flux as the initial ensemble spread. The sensitivity of the initial ensemble spread to $CH_4$ flux estimation is discussed in Section 4.2. The uncertainty to perturb prior fluxes is generated based

on random positive values with normal distribution. The monthly scale prior emission is linearly interpolated at 6 hourly intervals to be used in the MIROC4-ACTM simulation for data assimilation. This study performs two LETKF data assimilation experiments. In these experiments, we provided initial perturbation on regional basis over land (53 different land regions; Chandra et al., 2021) and at every grid over ocean, no spatial error correlation between grid points is considered among ensemble members. However, in Section 4.2.5, we also discussed the sensitivity of $CH_4$ data assimilation by providing initial ensemble spread at every grid by considering horizontal spatial error correlation between grid points among ensemble members, with a global mean correlation of 20%.

### 3.3 Experiment 1: Synthetic dense observation formulation

The OSSE setting with very accurate and dense observation surface data is an attempt to demonstrate that data assimilation system works reasonably in the estimation of the true surface flux. Errors in the estimated flux could arise due to the insufficient ensemble size and also the implemented inflation methods to overcome the under-sampling, along with simplified forecast process of emissions. In real data assimilation, there are additional sources of potential errors, such as, atmospheric transports, and inappropriate prior or observation uncertainties. In our OSSEs, $CH_4$ fluxes as mentioned in Section 3.2 are used as "true" fluxes in generating synthetic observations ($CH_4$ concentrations). In the experiment 1, the simulated surface layer $CH_4$ concentrations at each grid for the entire globe were used as synthetic assimilated observations. We added a constant measurement uncertainty of 5 ppb, which is typically achieved by the present-day measurement systems (e.g., Dlugokencky et. al, 2020).

In this study, the $CH_4$ observations are assimilated by applying the observation error covariance localization (Kotsuki et al., 2020) to reduce the spurious spatial correlation due to smaller ensemble size than the degrees of freedom of the system ($R \leftarrow R \times \exp\left(-\frac{1}{2}\{(d_h/\sigma_h)^2 + (d_v/\sigma_v)^2\}\right)$). Where $d_h$ and $d_v$ denote the horizontal distance (km) and vertical difference (log[Pa]) between the analysis model grid point and observation location. The tunable parameters $\sigma_h$ and $\sigma_v$ are the horizontal localization scale (km) and vertical localization scale (log[Pa]), respectively. Using the spatial localization technique, we have estimated the $CH_4$ flux for each grid by choosing the $CH_4$ observations that influence the grid point using optimal cutoff radius ($\simeq 3.65\sigma_{h,v}$; Miyoshi et al., 2007) with horizontal covariance localization ($\sigma_h$) of 2200 km and vertical covariance localization ($\sigma_v$) of 0.3 in the natural logarithmic pressure (log[Pa]) coordinate. The localization is performed to improve the signal to noise ratio of ensemble-based covariance. Numerous sensitivity experiments have been performed by varying the horizontal and vertical localization length in order to obtain the optimized $CH_4$ flux that best compare with the truth. The LETKF assimilates the observations within the specified radius to solve the analysis state at each grid point independently (Liu et al., 2016). State vector of the analysis includes the atmospheric $CH_4$ concentration, which is the prognostic variable of forecast model and the state vector is further augmented by surface $CH_4$ flux, which is not a model

prognostic variable. This augmentation enables the LETKF to directly estimate the parameter through the background error covariance with observed variables (Baek et al., 2006). The state vector augmentation is implemented similar to that used by Miyazaki et al. (2011). This approach analyses $CH_4$ flux during the analysis step. The purpose of the simultaneous $CH_4$ emission and concentration optimization is to reduce the uncertainty of the initial $CH_4$ concentrations on the $CH_4$ evolution during the assimilation window and to maximize the observations potential (Tian et al., 2014).

The atmospheric $CH_4$ concentration is changed during both the analysis and forecast steps. A challenge of this scheme is that, the analysis increment is added to the model state at each analysis step, without considering the global total $CH_4$ mass conservation in the model, but consistent with the observed local $CH_4$ abundance.

In this case, surface flux at every model grid point is analyzed with 8-days assimilation window during the year 2010 with the 100 ensemble members. The ensemble size and assimilation window are chosen based on the $CH_4$ flux estimation accuracy calculated by performing sensitivity experiment for ensemble size (60, 80, and 100) and assimilation window (3-days and 8-days), respectively (not shown).

### 3.4 Experiment2: synthetic satellite observation formulation

One way to address the real-world $CH_4$ flux estimation problem is to first make the OSSE dataset like real observations. In this OSSE experiment, we have assimilated synthetic column average $CH_4$ concentrations with a coverage mimicking GOSAT satellite observations. We prepared a model simulated column averaged $CH_4$ concentrations ($XCH_4$) dataset that is spatiotemporally sampled with GOSAT observations as follows:

$$\mathrm{XCH_4} = \mathrm{XCH_{4(a\ priori)}} + \sum_j h_j\, a_j (\mathrm{CH_{4(ACTM)}} - \mathrm{CH_{4(a\ priori)}})_j \qquad (10)$$

Where, $XCH_4$ is the column-averaged model simulated $CH_4$ concentration. $\mathrm{XCH_{4(a\ priori)}}$ is a priori column-averaged concentration. $\mathrm{CH_{4(ACTM)}}$ and $\mathrm{CH_{4(a\ priori)}}$ are the $CH_4$ profile from ACTM and a priori, respectively. $h_j$ is the pressure weighting function (j is the vertical layer index), and $a_j$ represents averaging kernel matrix for the column retrieval which is the sensitivity of the retrieved total column at the various ('j') atmospheric levels. In the next step, we added the same retrieval ($XCH_4$) error as GOSAT to the $XCH_4$ (ACTM simulated) to make the OSSE more realistic and then attempt to estimate the true fluxes.

In this case, the $CH_4$ flux has been estimated for each grid by choosing the $CH_4$ observation with cutoff radius ($\simeq 3.65\ \sigma_{h,v}$) with horizontal covariance localization ($\sigma_h$) of 5000 km and vertical covariance localization ($\sigma_v$) of 0.35 in the natural logarithmic pressure (log[Pa]) coordinate. The

optimal horizontal and vertical covariance localization values are chosen based on trial and error method (those best fits to estimate $CH_4$ flux when compared with truth). A long cutoff radius has been chosen due to sparse observational coverage of GOSAT. The surface flux is analyzed at every model grid point with 8-days assimilation window and 100 ensemble members those are chosen based on sensitivity experiments discussed in Section 4.2.

## 4. Results and Discussion

### 4.1 Experiment with dense OSSE

The time series of normalized RMSE ($\sqrt{\sum_{i=1}^{n}(x_i^a - x_i^t)^2/n}/\tilde{x}^t$ ; $x_i^a$ and $x_i^t$ is the analysis and true state at *i*th model grid point, n is the total number of grid points, and $\tilde{x}^t$ represents the mean of true flux) in the analyses over global landmass region is shown in Figure 2. The normalized global RMSE is calculated using FM and RTPS inflation methods (Fig. 2) after assimilating synthetic observation at every grid (Section 3.4). Noteworthy is that the experiment with FM inflation method shows 10-15% larger error in estimating the atmospheric surface $CH_4$ flux compared to RTPS inflation method. One of the reasons of better RMSE using RTPS inflation method is due to the more degrees of freedom provided by relaxation ($\alpha_{RTPS}$) in ensemble spread (Eq. 8) that could nudge the ensemble of $CH_4$ concentrations towards observations. The initial flux analysis spread using RTPS and FM is shown in supporting information (Fig. S1) which shows larger initial analysis flux spread over Brazil, tropical America, and Asia in RTPS inflation compared to FM inflation method. We performed numerous sensitivity test with RTPS inflation method and found that uniform relaxation is not substantial, for some of the regions. Figure 2 shows the RMSE for FM, fixed RTPS ($\alpha_{RTPS} = 0.4$, applied globally, the optimized value is obtained by manual fine tuning) and conditional RTPS ( $\alpha_{RTPS}$= 0.3-0.7 applied different $\alpha_{RTPS}$ regionally by manual fine tuning). We find that the conditional RTPS method improves the accuracy by ~5% compared to fixed RTPS and 10-15% compared to FM.

We have also shown RMSE (not normalized) of surface flux in supplementary information (Fig. S2). Flux RMSE has been estimated globally for both the inflation methods, and also for south of 20°N (by considering only those land grids which fall into south of 20°N; Fig. S2) for comparative purposes. It could be noticed that (supporting information Fig. S2), above north of 20°N, the flux estimation error is higher, specifically during spring-summer when $CH_4$ emissions peak over most of the northern hemispheric regions (Fig. 3). The high uncertainty during spring-summer (Fig. S2) in the flux estimation over these regions could appear due to the attenuation of surface observations as a result of active vertical mixing. The RMSE during autumn (Fig. S2) is comparable in case of global and south of 20°N, which indicates RMSE arising from southern hemispheric regions, likely over Brazil as it peaks during autumn (Fig. 3).

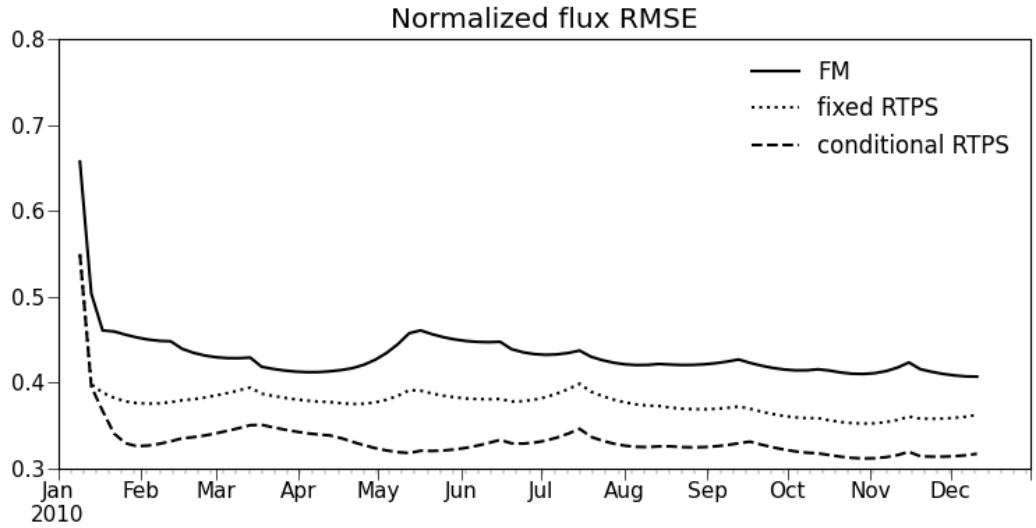


299

300 **Figure 2.** Time series of normalized RMSE of surface $CH_4$ flux analysis, for 1 year of data
301 assimilation using FM, fixed RTPS, and conditional RTPS inflation methods over global landmass
302 region.

303 Figure 3 shows regional total flux seasonal cycles comparison of the estimated fluxes for 15 terrestrial
304 regions with those of the prior and true fluxes. The estimated flux retrieved using RTPS inflation
305 method over different regions agrees well with that of true flux. We intend to show the capability of
306 LETKF estimated fluxes over these regions using surface observations to mimic the true fluxes in our
307 understanding of terrestrial biosphere $CH_4$ cycle. These results are consistent with Figure 2 with
308 annual global normalized mean bias ($\sum_{i=1}^{n}(x_i^a - x_i^t)/\sum_{i=1}^{n}(x_i^t)$) of -0.04. It could also be noticed
309 from Figure 3 that estimated fluxes converge to true fluxes over most of the regions after about 2-3
310 months.

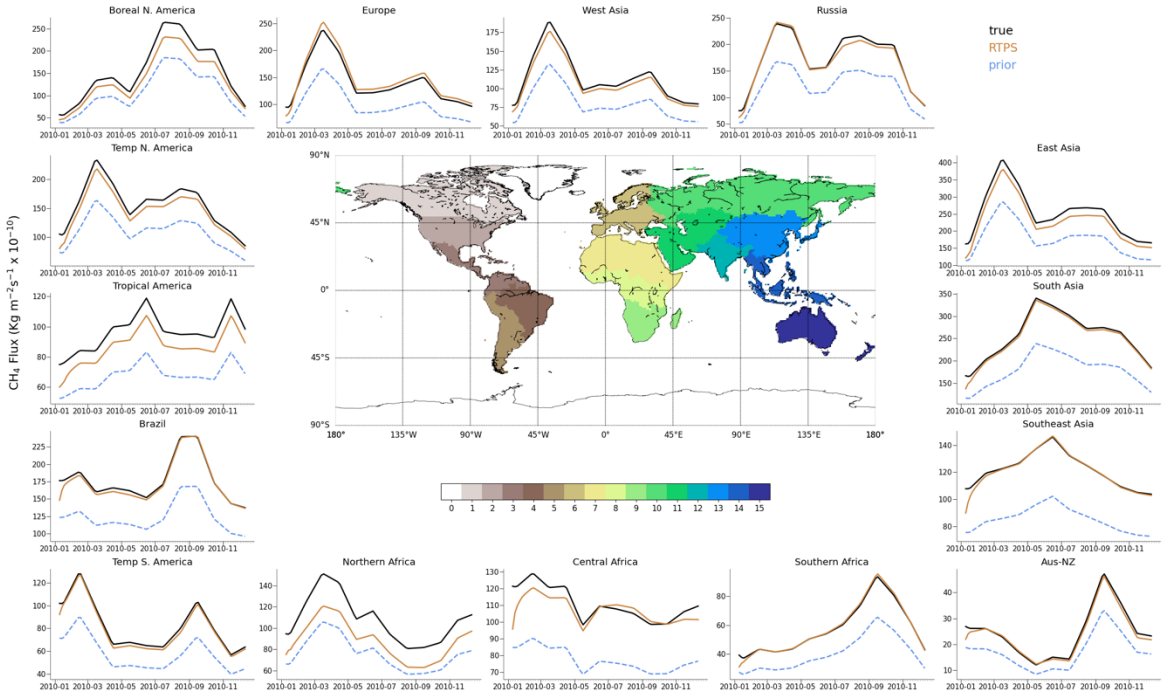


311

312 **Figure 3.** The 1-year $CH_4$ total flux seasonal cycles of true (black), prior (blue), and estimated from
313 the LETKF (orange) RTPS inflation method in 15 regions after assimilating dense synthetic surface
314 $CH_4$ observations.

315 To see the degree of similarity in the flux distribution between the estimated and true fluxes, we show
316 monthly mean spatial flux distribution for June, and November in Figure 4 and 5, respectively, along
317 with the bias in prior and estimated flux. As shown in Figures 4 and 5, the general spatial patterns of
318 the true flux are estimated well. These results suggest that, our LETKF system is capable of
319 reproducing continental spatial flux patterns by using such an idealized dense surface observational
320 data. However, some clear differences in flux estimation could be noticed from FM and RTPS
321 inflation method (Figs. 4 and 5), for e.g., over Eurasian and American continent, analysis with RTPS
322 shows clear improvement compared to FM covariance inflation method. We calculated the global
323 mean normalized bias with RTPS and FM covariance inflation method which is found to be -0.04 and
324 -0.11, respectively over land regions that shows RTPS significantly improved the flux estimation
325 compared to FM covariance inflation method.

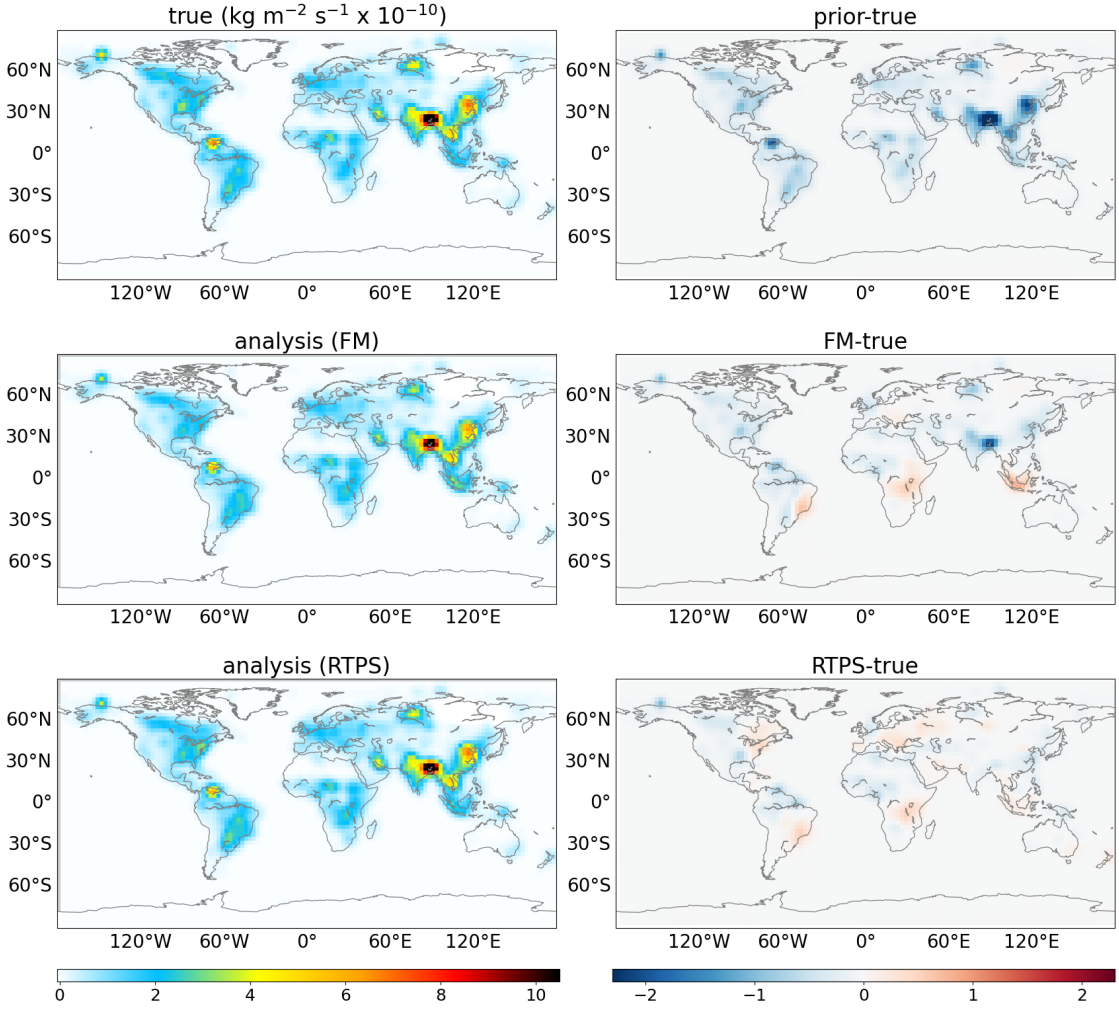


326

327 **Figure 4.** Spatial distribution of surface $CH_4$ fluxes (true; top left panel, FM analysis; middle left
328 panel, RTPS analysis; bottom left panel) and the associated bias in prior (prior-true; top right panel)
329 and estimated (FM-true; middle right panel, RTPS-true; bottom right panel) fluxes during June, 2010.

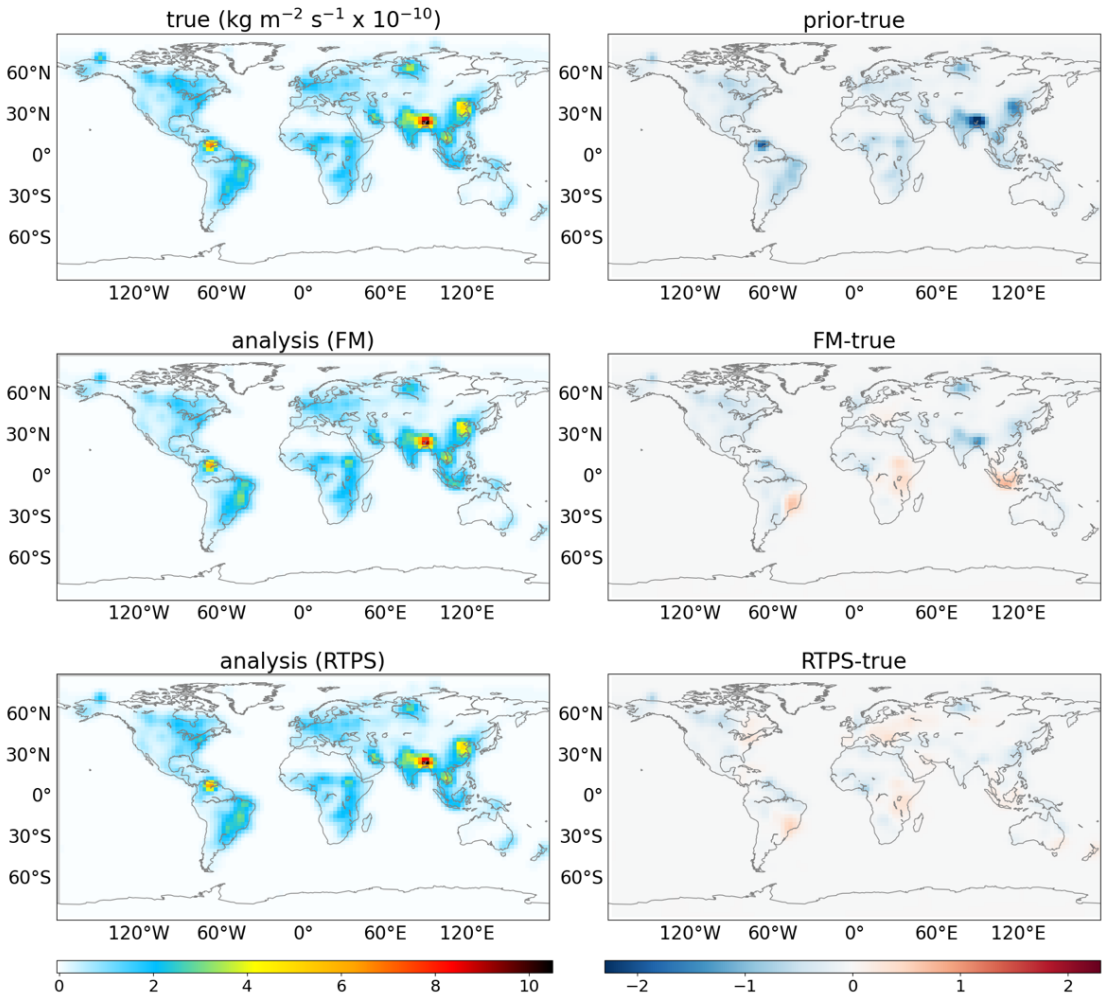


**Figure 5.** Same as Figure 4 but for November, 2010.

### 4.2 Experiment by mimicking the real satellite observational data set

In this section we discuss the LETKF flux estimation by assimilation of GOSAT synthetic $CH_4$ concentration observations. Figure 6 shows the model simulated mean $XCH_4$ concentration sampled spatiotemporally with GOSAT observations during January and July for the year 2010 (sampling method discussed in Section 3.4). In this case we have shown different LETKF sensitivity experiments such as; LETKF sensitivity to (1) FM, RTPS, adaptive multiplicative inflation (2) assimilation window (3) ensemble size, (4) chi-square test, (5) prior ensemble spread. In the LETKF sensitivity experiments from 1-4, the initial ensemble spread provided similar way as Experiment 1.

#### 4.2.1 LETKF sensitivity to FM, RTPS, and adaptive multiplicative inflation

This study mainly emphasizes on FM and RTPS inflation methods used in $CH_4$ LETKF data assimilation. The annual average normalized RMSE (absolute bias) with RTPS and FM covariance inflation is found to be 0.59 (0.18) and 0.64 (0.22), respectively. The RTPS inflation method performs

better than the FM inflation method overall. In addition to RTPS inflation, sensitivity test is also performed using adaptive multiplicative inflation methods.

In the adaptive inflation, we need to provide an initial multiplicative inflation factor at the beginning of data assimilation cycle (Cycle 1 in Fig. 1). Following the method of Deroziers et al. (2005), the multiplication inflation factor information calculated in previous cycle (i.e. Cycle1 in Fig. 1) is used for next data assimilation cycle at every grid point (Cycle 2 in Fig. 1). We perform two sensitivity experiments. In the first (second) case we provided 50% (40%) initial inflation in the beginning of Cycle 1 (Fig. 1). The normalized RMSE in the both the adaptive inflation sensitivity experiments are comparable (0.65, Supporting information Fig. S3a) till July, but from the beginning of August, RMSE increases exponentially in the first experiment. However, in terms of chi-square distribution $CH_4$ flux estimation with first sensitivity adaptive multiplicative inflation experiment (50% initial inflation case) is better than second sensitivity experiment (Supporting information Fig. S3b; chi-square test described in Section 4.2.4). To identify the regions of high estimated $CH_4$ flux error, we have shown the background error spread in $CH_4$ flux estimation over 15 regions (Supporting information Fig. S3c) and found that spread over west and south east Asia rises exponentially post July that indicates the rise of estimated $CH_4$ flux error over these regions in the first sensitivity adaptive multiplicative inflation experiment. Our analysis suggests that $CH_4$ flux estimation is depending on the initial inflation factor provided in the beginning of data assimilation cycle (Cycle 1, Fig. 1) in adaptive multiplication method. Also, we need to be very careful to monitor the background error spread evolution with time to estimate the $CH_4$ flux with adaptive inflation, chi-square distribution analysis is not sufficient.

In case of RTPP inflation, we found the parameter $\alpha_{RTPP}$ is very difficult to fine-tuned due to its very high sensitivity to estimate the $CH_4$ flux. We fail to obtain an optimized $\alpha_{RTPP}$ value to estimate the $CH_4$ flux. Whitaker & Hamill, 2012, also demonstrated the better accuracy in LETKF meteorological data assimilation with RTPS compared to RTPP covariance inflation method. They found RTPP method produces very large errors if the inflation parameter exceeds the optimal value.

**4.2.2 Assimilation window**

The LETKF data assimilation window length determines the time span of the observations assimilated in each assimilation cycle. We have shown the sensitivity of two assimilation window size configurations; 3 days and 8 days in supporting information Figure S4. Our sensitivity experiments with window size configurations show that 8 days long assimilation window estimates the $CH_4$ flux with better accuracy (~10%) compared to 3 days assimilation window, because more observational information is incorporated into the system with 8 days long assimilation window. This study uses 8 days assimilation window for $CH_4$ LETKF data assimilation.

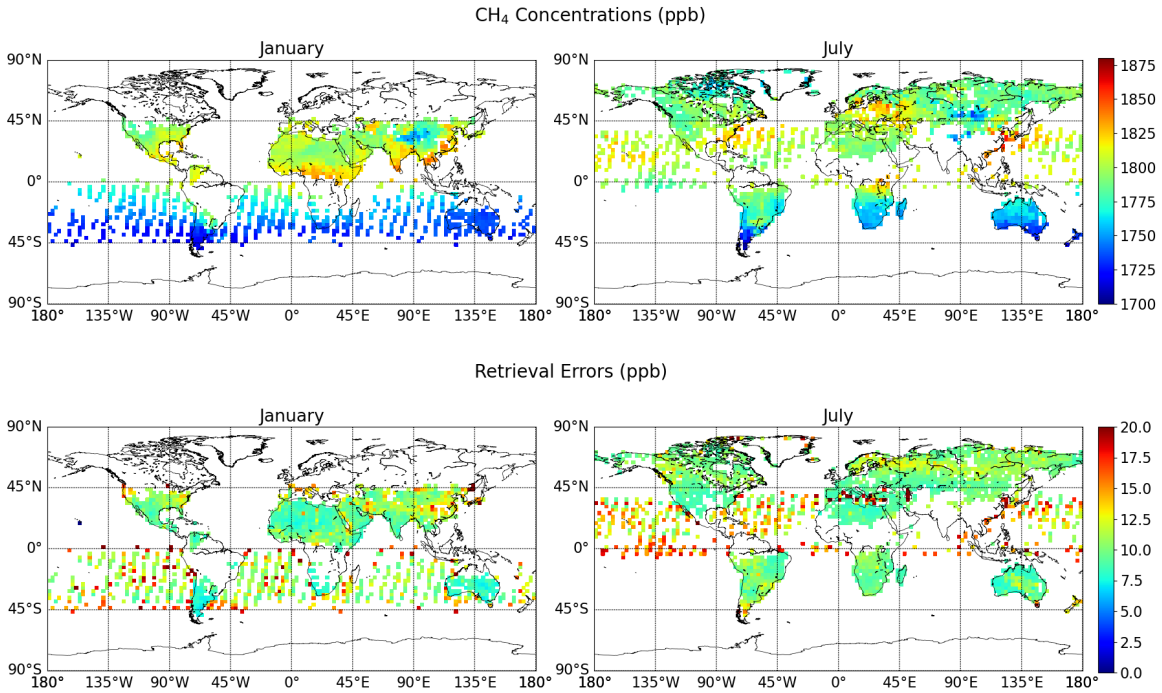


**Figure 6.** Monthly mean ACTM simulated $XCH_4$ (ppb) sampled with GOSAT observations to be assimilated (valid during the year 2010). The actual retrieval errors are added in the synthetic GOSAT observations. Data are shown for two representative months, depicting the southern and northern hemisphere differences in data coverage.

### 4.2.3 Ensemble size

Figure 7a shows the RMSE using different ensemble members. The optimal $\alpha_{RTPS}$ (Eq. 8) value ranging from 0 to 1, is applied based on flux estimation accuracy achieved by fine tuning $\alpha_{RTPS}$ value over different regions. The RMSE stabilizes gradually as the ensemble size increases from 60 to 80 to 100 ensemble members. The ensemble size dependency of flux estimation suggests the further scope of the improvement in flux estimation by increasing the ensemble members. In this study we stick to 100 ensemble members due to high computational cost while solving large covariance matrices. The larger error in flux estimation in case of column averaged synthetic GOSAT $CH_4$ observations assimilation compared to dense observations (Fig. 2) is likely due to the weaker constraint on surface fluxes provided by satellite observations and sparse observations.

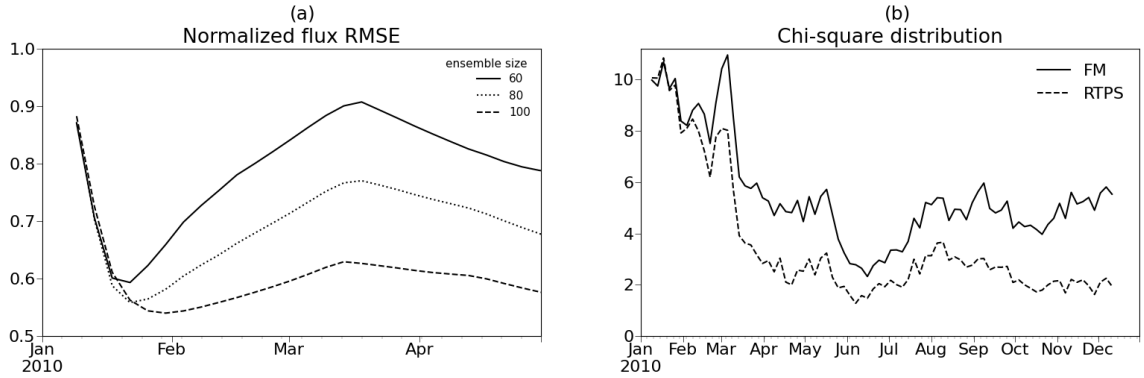


**Figure 7:** (a) Flux estimation RMSE using different ensemble size with RTPS covariance inflation. (b) Chi-square distribution using FM and RTPS covariance inflation methods with the ensemble size of 100.

#### 4.2.4 Chi-square test

We have carried out chi-square test for the evaluation of background error covariance matrix (Miyazaki et al., 2012). For the $\chi^2$ test, the innovation statistics are diagnosed from the observation minus forecast $(y^o - Hx^b)$, the estimated error covariance in the observation space ($HP^bH^T + R$), and the number of observations k, such as:

$$Y = \frac{1}{\sqrt{k}}\left(HP^bH^T + R\right)^{-1/2}\left(y^o - Hx^b\right) \quad (11)$$

Using this statistic, the $\chi^2$ is defined as follow:

$$\chi^2 = \mathrm{trace}YY^T \quad (12)$$

The performance of background error covariance matrix determined based on the high and lower value of chi-square. Chi-square value should converge to 1, a value higher (lower) than 1 indicates underestimation (overestimation) of the background error covariance matrices. Our results suggest that, background error covariance matrix is highly underestimated in both RTPS and FM covariance inflation methods (Fig. 7b). However, the chi-square values convergence towards 1 is better in the case of RTPS compared to FM covariance inflation method which indicates the improved representation of background errors and then more appropriate data assimilation corrections in the case of the RTPS inflation method. The chi-square distribution starts saturating after the month of March. Post March analysis shows the background error covariance matrix underestimation is much higher (>100%) in case of FM compared to RTPS covariance inflation method.

#### 4.2.5 $CH_4$ LETKF sensitivity to initial ensemble spread

A test case for $CH_4$ LETKF data assimilation has been performed where the initial spread is provided by considering the initial perturbation on each model grid with spatial error correlation between grid points among ensemble members, with global mean correlation of 20%. In this case, we found that the analysis fluxes are extremely sensitive to the initial ensemble spread if prior fluxes perturbed with more than 5% prior uncertainty. Therefore, we used initial ensemble perturbation with only 2% prior uncertainty. Reducing the initial ensemble spread reduces the $CH_4$ flux estimation sensitivity (>60%). However, it also poses a challenge to mitigate the under-dispersive background error covariance matrix. We performed LETKF data assimilations in this case with RTPS covariance inflation method ($\alpha_{RTPS}$ = 0.9 optimized value is used here uniformly) with 8-days long assimilation window and 100 ensemble members and calculated the normalized RMSE between analysis and true fluxes (Supporting information Fig. S5). Noteworthy that, the estimated error between analysis and true fluxes (Fig. S5) with this setting (grid-wise initial ensemble spread) is still larger (25%) than the case when region-wise initial ensemble spread provided (Fig. 7a; 100 ensemble size). It suggests that, initial ensemble spreads among ensemble members needs to be carefully provided that best represents $CH_4$ variability among ensembles to estimate the $CH_4$ flux.

#### 4.2.6 Estimated $CH_4$ flux analysis

Figure 8 shows the regional fluxes seasonal cycle comparison for the estimated fluxes over 15 terrestrial regions with those of the prior and true fluxes. We have also shown assimilation results in case of FM inflation method in supporting information (Fig. S6), which shows the flux estimation disagreement over more regions compared to RTPS inflation method; e.g., for Tropical and North America, whole African continent, Australia-New Zealand.

We have shown the GOSAT observations in Figure 6 and supporting information Figure S7. We found very marginal flux estimation improvement over Central Africa after May (Fig. 8), that could be associated with the less GOSAT coverage over this region (Fig. 6). On the other hand, over Northern Africa, no improvement in flux estimation is found. In case of dense OSSE too (Fig. 3), we didn't find satisfactory flux estimation over Northern Africa which is most probably related to the insufficient initial spread among ensemble members over this region (we have used same initial ensemble spread in both OSSE cases). Over Europe, GOSAT observations are remarkably less, specifically for first few months (January-April; supporting information Fig. S7). Therefore, the flux update over Europe would be influenced by the observations from neighboring regions falling under the chosen cutoff radius that are mainly in Northern Africa where the flux estimation itself not satisfactory. It could also be noticed that the retrieval error added in this OSSE case are high over Europe (September-October; supporting information Fig. S7),) and its adjacent Sea (Mediterranean Sea; June-August) which could also affect the surface $CH_4$ flux estimation.

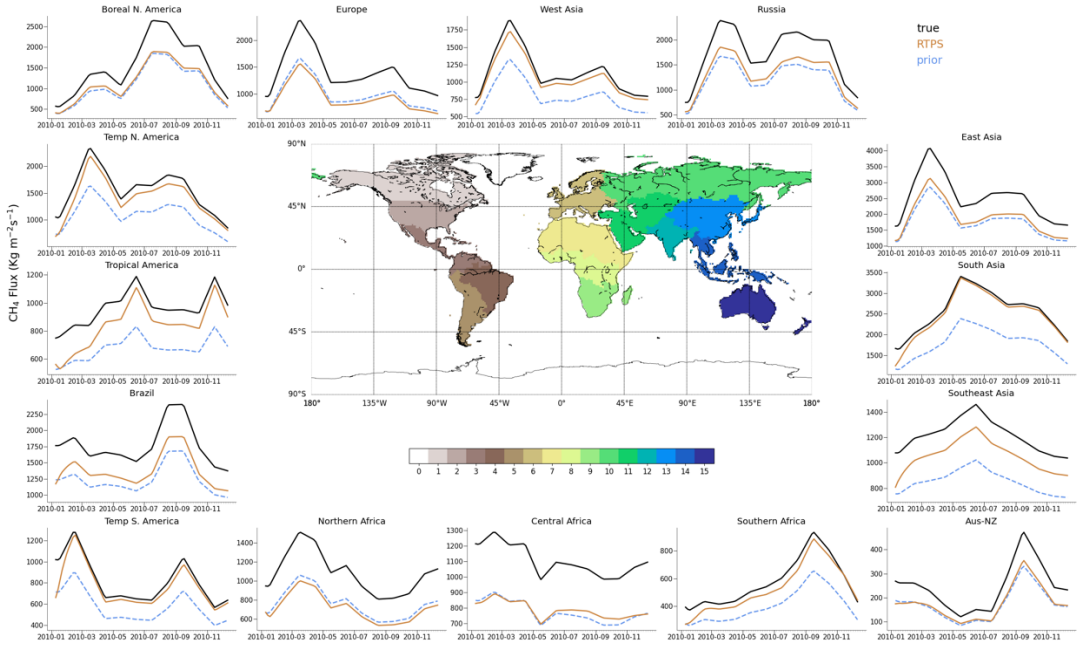


**Figure 8.** Same as Figure3 but after assimilating synthetic GOSAT observations.

Figure 9 and 10 show spatial patterns of the true and estimated fluxes by assimilating the column averaged $CH_4$ concentrations during June and November (Fig. 6). It may be noticed that RTPS covariance inflation method better able to estimate the true flux pattern compared to FM covariance inflation method. The spatial pattern shown using RTPS inflation method emphasizes the positive and negative bias in the estimated flux (Figs. 9 and 10), but generally agrees with the flux seasonal cycle plots shown in Figure 8.

Our LETKF $CH_4$ data assimilation experiment by assimilating GOSAT synthetic observation with the implementation of the advanced RTPS covariance inflation method better estimate the time-evolving surface $CH_4$ fluxes compared to FM covariance inflation method. The difficulty to estimate the surface $CH_4$ flux over a few regions may be overcome by applying additional methodologies, such as the assimilation of surface observations simultaneously, and the use of information about the $CH_4$ fluxes climatology. A correction factor derived based on empirical formulation that could use $CH_4$ flux climatology information is needed to apply to maintain the $CH_4$ mass conservation. This could be implemented by the checking the simulated $CH_4$ burden gain between years in comparison with the observed $CH_4$ growth rates.

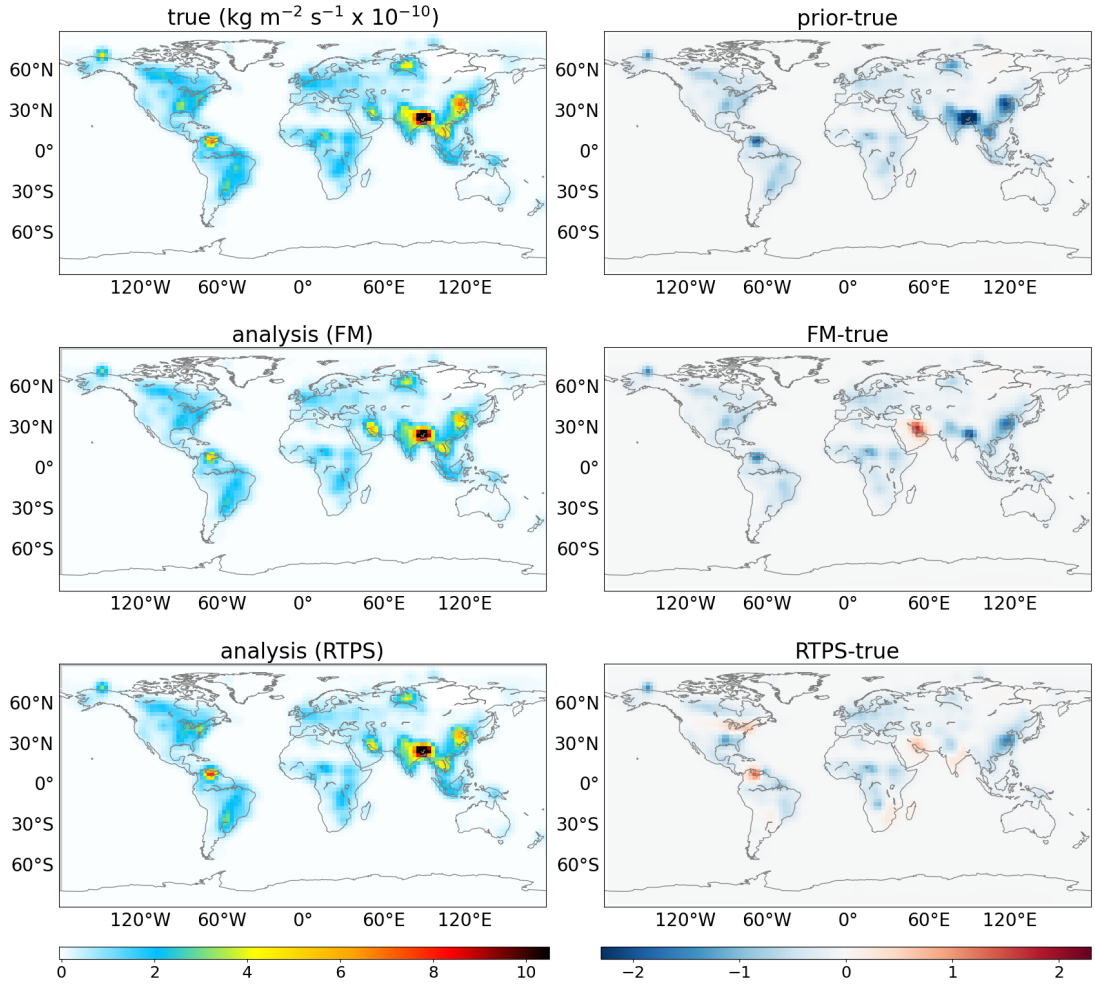


465

466 **Figure 9.** Monthly mean true (true; top left panel) and estimated (FM analysis; middle left panel,
467 RTPS analysis; bottom left panel) $CH_4$ flux after assimilating column averaged synthetic $CH_4$
468 concentrations (Fig. 6) during June using FM and RTPS inflation methods. The associated bias with
469 prior and estimated fluxes is also shown (prior-true; top right panel; FM-true; middle right panel,
470 RTPS-true; bottom right panel).

471

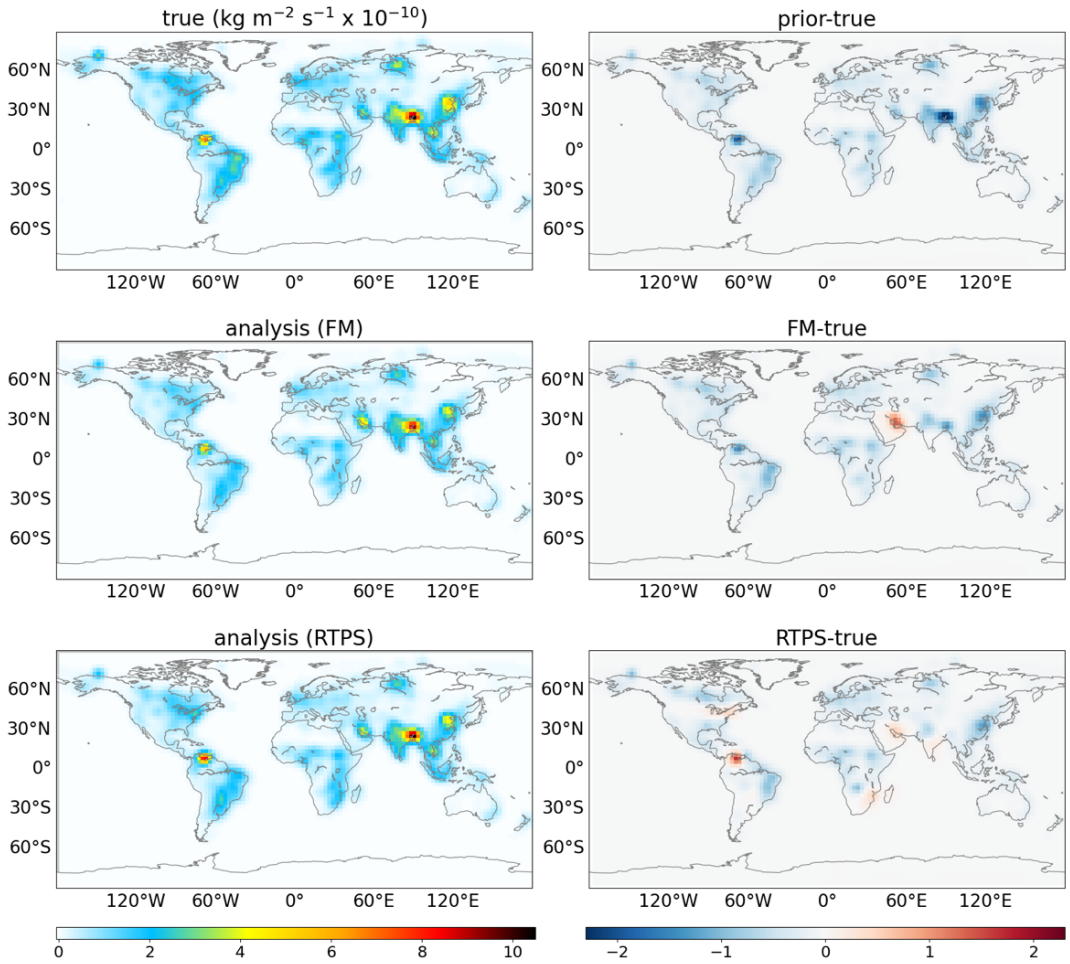


**Figure 10.** Same as Figure 9 but for November.

## 5. Summary

In this study, we have introduced 4D-LETKF data assimilation system that utilizes MIROC4-ACTM as a forward model for $CH_4$ flux estimation. This study has extensively tested both FM and RTPS inflation methods for the LETKF $CH_4$ flux estimation. We have conducted two experiments to demonstrate the ability of LETKF system to estimate the $CH_4$ surface flux globally. In Experiment1, we have assimilated the synthetic dense surface $CH_4$ observations. While in Experiment2, synthetic GOSAT $CH_4$ observations are assimilated. Based on the results of the sensitivity tests using FM and RTPS inflation methods in Experiment1, we have found that RTPS inflation produces significantly less normalized RMSE (10-15%) compared to FM inflation method. In Experiment2, we discussed, LETKF parameters such as, different inflation techniques, ensemble size, assimilation window, initial ensemble spread sensitivity, and chi-square test. The ensemble size (this study uses maximum 100 ensemble members) sensitivity test suggests that more ensemble members could help to accurately represent the covariance matrix with more degrees of freedom. The assimilation window sensitivity

test exhibits that 8 days assimilation window reduces the normalized flux RMSE by about 10% compared to 3 days assimilation window in case of GOSAT synthetic observations assimilation.

Our approach of assimilation with RTPS inflation could provide more degrees of freedom to fit the ensemble of $CH_4$ concentrations to the observed ones, resulting the improved analyzed fluxes. The RTPS inflation method is capable of obtaining reasonable flux estimates with normalized annual mean bias of 0.04, and 0.61 in case of dense surface synthetic observations and GOSAT synthetic observations, respectively. We demonstrated in our sensitivity OSSE experiment with synthetic GOSAT observations that, over American and African continents and also over Australia - New Zealand, the LETKF data assimilation with FM inflation method does not show much improvement in the true flux estimation, but RTPS inflation method reasonably estimate the true flux over most of these regions. One of the reasons for better flux estimates from RTPS inflation method is the prevention of analysis spread drastically. In the $CH_4$ LETKF flux estimation, surface $CH_4$ flux is not a prognostic state vector in the ACTM, which results in the decay of spread continuously in analysis steps. RTPS inflation method could mitigate such under disperse spread problem. This study finds that spatially homogeneous relaxation is not sufficient. It needs to be fine-tuned and applied conditionally.

The sensitivity of LETKF $CH_4$ flux estimation to initial ensemble spread needed to be carefully dealt with when applied to real data assimilation system. A future OSSE with additive covariance inflation technique could be interesting while applied with RTPS inflation method for $CH_4$ LETKF data assimilation since in additive covariance inflation initial estimated flux error cannot propagate. The state vector augmentation technique used here updates the flux after each data assimilation cycle but it doesn't conserve the total atmospheric $CH_4$ amount which is one of the limitations of this work. A correction factor needs to be implemented to conserve the total atmospheric $CH_4$ amount after completion of a few data assimilation cycles. We have not accounted for the transport error due to meteorological fields in this work (Patra et al., 2011b), in case of real observations data assimilation a week-long window may introduce transport errors in $CH_4$ analysis because of nonlinear growth of ensemble perturbations.

*Code and data availability.* The LETKF source codes can be accessed from https://doi.org/10.5281/zenodo.7127658. All the scripts for running the LETKF data assimilation software, input and output results data files are available at https://doi.org/10.5281/zenodo.7098323. $CH_4$ ACTM simulation module coupled with MIROC4-AGCM can be accessed from https://doi.org/10.5281/zenodo.7118365. The source code of MIROC4-AGCM is archived at https://doi.org/10.5281/zenodo.7274240 with restriction because of the copyright policy of the MIROC developer community, and no contribution of this work to the MIROC4 source code development.

*Author contributions.* The LETKF data assimilation experiments were designed by JSHB. PKP, MT and TS help to set the LETKF code on MIROC4-ACTM for $CH_4$ data assimilation. The manuscript is prepared by JSHB and analysis interpretation input and feedback are provided by PKP, TS, KM. All coauthors, KM, TS, PKP, NS, MT and YK contributed to writing and revision of the paper.

*Acknowledgements.* This research was performed by the Environment Research and Technology Development Fund (JPMEERF20182002) of the Environmental Restoration and Conservation Agency of Japan and GOSAT-GW project fund. We also thank to Ryu Saito for the initial set-up of LETKF code on MIROC4-ACTM for $CH_4$.

## References

Anderson, J. L. and Anderson, S. L.: A Monte Carlo Implementation of the Nonlinear Filtering Problem to Produce Ensemble Assimilations and Forecasts, Mon. Weather Rev., 127, 2741–2758, https://doi.org/10.1175/1520-0493(1999)127<2741:AMCIOT>2.0.CO;2, 1999.

Baek, S.-J., Hunt, B. R., Kalnay, E., Ott, E., and Szunyogh, I.: Local ensemble Kalman filtering in the presence of model bias, Tellus A Dyn. Meteorol. Oceanogr., 58, 293–306, https://doi.org/10.1111/j.1600-0870.2006.00178.x, 2006.

Bisht, J. S. H., Machida, T., Chandra, N., Tsuboi, K., Patra, P. K., Umezawa, T., Niwa, Y., Sawa, Y., Morimoto, S., Nakazawa, T., Saitoh, N., and Takigawa, M.: Seasonal Variations of SF 6 , CO 2 , CH 4 , and N 2 O in the UT/LS Region due to Emissions, Transport, and Chemistry, J. Geophys. Res. Atmos., 126, https://doi.org/10.1029/2020JD033541, 2021.

Bruhwiler, L., Dlugokencky, E., Masarie, K., Ishizawa, M., Andrews, A., Miller, J., Sweeney, C., Tans, P., and Worthy, D.: CarbonTracker-CH4: an assimilation system for estimating emissions of atmospheric methane, Atmos. Chem. Phys., 14, 8269–8293, https://doi.org/10.5194/acp-14-8269-2014, 2014.

Cao, M., Marshall, S., and Gregson, K.: Global carbon exchange and methane emissions from natural wetlands: Application of a process-based model, J. Geophys. Res. Atmos., 101, 14399–14414, https://doi.org/10.1029/96JD00219, 1996.

Chandra, N., Patra, P. K., Bisht, J. S. H., Ito, A., Umezawa, T., Saigusa, N., Morimoto, S., Aoki, S., Janssens-Maenhout, G., Fujita, R., Takigawa, M., Watanabe, S., Saitoh, N., and Canadell, J. G.: Emissions from the Oil and Gas Sectors, Coal Mining and Ruminant Farming Drive Methane Growth over the Past Three Decades, J. Meteorol. Soc. Japan. Ser. II, 99, 309–337, https://doi.org/10.2151/jmsj.2021-015, 2021.

554 Daley, R.: The lagged-innovation covariance: A performance diagnostic for data assimilation, Mon.
555 Wea. Rev., 120, 178–196, 1992.

556 Desroziers, G., Berre, L., Chapnik, B., and Poli, P.: Diagnosis of observation, background and
557 analysis-error statistics in observation space, Q. J. R. Meteorol. Soc., 131, 3385–3396,
558 https://doi.org/10.1256/qj.05.108, 2005.

559 Dlugokencky, E. J., Crotwell, A. M., Mund, J. W., Crotwell, M. J., & Thoning, K. W.: Atmospheric
560 Methane Dry Air Mole Fractions from the NOAA GML Carbon Cycle Cooperative Global Air
561 Sampling Network, 1983-2019, Version: 2020-07, https://doi.org/https://doi.org/10.15138/VNCZ-
562 M766, 2020.

563 Enting, I. G.: Inverse Problems in Atmospheric Constituent Transport, Cambridge University Press,
564 https://doi.org/10.1017/CBO9780511535741, 2002.

565 Fung, I., John, J., Lerner, J., Matthews, E., Prather, M., Steele, L. P., and Fraser, P. J.: Three-
566 dimensional model synthesis of the global methane cycle, J. Geophys. Res., 96, 13033,
567 https://doi.org/10.1029/91JD01247, 1991.

568 Houtekamer, P. L. and Zhang, F.: Review of the Ensemble Kalman Filter for Atmospheric Data
569 Assimilation, Mon. Weather Rev., 144, 4489–4532, https://doi.org/10.1175/MWR-D-15-0440.1,
570 2016.

571 Houweling, S., Kaminski, T., Dentener, F., Lelieveld, J., and Heimann, M.: Inverse modeling of
572 methane sources and sinks using the adjoint of a global transport model, J. Geophys. Res. Atmos.,
573 104, 26137–26160, https://doi.org/10.1029/1999JD900428, 1999.

574 Hunt, B. R., Kostelich, E. J., and Szunyogh, I.: Efficient data assimilation for spatiotemporal chaos: A
575 local ensemble transform Kalman filter, Phys. D Nonlinear Phenom., 230, 112–126,
576 https://doi.org/10.1016/j.physd.2006.11.008, 2007.

577 Ito, A.: Methane emission from pan-Arctic natural wetlands estimated using a process-based model,
578 1901–2016, Polar Sci., 21, 26–36, https://doi.org/10.1016/j.polar.2018.12.001, 2019.

579 Janssens-Maenhout, G., Crippa, M., Guizzardi, D., Muntean, M., Schaaf, E., Dentener, F.,
580 Bergamaschi, P., Pagliari, V., Olivier, J. G. J., Peters, J. A. H. W., van Aardenne, J. A., Monni, S.,
581 Doering, U., Petrescu, A. M. R., Solazzo, E., and Oreggioni, G. D.: EDGAR v4.3.2 Global Atlas of
582 the three major greenhouse gas emissions for the period 1970–2012, Earth Syst. Sci. Data, 11, 959–
583 1002, https://doi.org/10.5194/essd-11-959-2019, 2019.

584 Kalnay, E. and Yang, S.-C.: Accelerating the spin-up of Ensemble Kalman Filtering, Q. J. R.

585 Meteorol. Soc., 136, 1644–1651, https://doi.org/10.1002/qj.652, 2010.

586 Kang, J.-S., Kalnay, E., Miyoshi, T., Liu, J., and Fung, I.: Estimation of surface carbon fluxes with an
587 advanced data assimilation methodology, J. Geophys. Res. Atmos., 117, D24101,
588 https://doi.org/10.1029/2012JD018259, 2012.

589 Kobayashi, S., Ota, Y., Harada, Y., Ebita, A., Moriya, M., Onoda, H., Onogi, K., Kamahori, H.,
590 Kobayashi, C., Endo, H., Miyaoka, K., and Takahashi, K.: The JRA-55 Reanalysis: General
591 Specifications and Basic Characteristics, J. Meteorol. Soc. Japan. Ser. II, 93, 5–48,
592 https://doi.org/10.2151/jmsj.2015-001, 2015.

593 Kotsuki, S., Ota, Y., and Miyoshi, T.: Adaptive covariance relaxation methods for ensemble data
594 assimilation: experiments in the real atmosphere, Q. J. R. Meteorol. Soc., 143, 2001–2015,
595 https://doi.org/10.1002/qj.3060, 2017.

596 Kotsuki, S., Pensoneault, A., Okazaki, A., and Miyoshi, T.: Weight structure of the Local Ensemble
597 Transform Kalman Filter: A case with an intermediate <scp>atmospheric general circulation
598 model</scp>, Q. J. R. Meteorol. Soc., 146, 3399–3415, https://doi.org/10.1002/qj.3852, 2020.

599 Liu, J., Bowman, K. W., and Lee, M.: Comparison between the Local Ensemble Transform Kalman
600 Filter (LETKF) and 4D-Var in atmospheric CO 2 flux inversion with the Goddard Earth Observing
601 System-Chem model and the observation impact diagnostics from the LETKF, J. Geophys. Res.
602 Atmos., 121, 13,066-13,087, https://doi.org/10.1002/2016JD025100, 2016.

603 Lorente, A., Borsdorff, T., Butz, A., Hasekamp, O., aan de Brugh, J., Schneider, A., Wu, L., Hase, F.,
604 Kivi, R., Wunch, D., Pollard, D. F., Shiomi, K., Deutscher, N. M., Velazco, V. A., Roehl, C. M.,
605 Wennberg, P. O., Warneke, T., and Landgraf, J.: Methane retrieved from TROPOMI: improvement of
606 the data product and validation of the first 2 years of measurements, Atmos. Meas. Tech., 14, 665–
607 684, https://doi.org/10.5194/amt-14-665-2021, 2021.

608 Maasakkers, J. D., Jacob, D. J., Sulprizio, M. P., Turner, A. J., Weitz, M., Wirth, T., Hight, C.,
609 DeFigueiredo, M., Desai, M., Schmeltz, R., Hockstad, L., Bloom, A. A., Bowman, K. W., Jeong, S.,
610 and Fischer, M. L.: Gridded National Inventory of U.S. Methane Emissions, Environ. Sci. Technol.,
611 50, 13123–13133, https://doi.org/10.1021/acs.est.6b02878, 2016.

612 Meirink, J. F., Bergamaschi, P., and Krol, M. C.: Four-dimensional variational data assimilation for
613 inverse modelling of atmospheric methane emissions: method and comparison with synthesis
614 inversion, Atmos. Chem. Phys., 8, 6341–6353, https://doi.org/10.5194/acp-8-6341-2008, 2008.

615 Miyazaki, K., Maki, T., Patra, P., and Nakazawa, T.: Assessing the impact of satellite, aircraft, and
616 surface observations on CO 2 flux estimation using an ensemble-based 4-D data assimilation system,

J. Geophys. Res., 116, D16306, https://doi.org/10.1029/2010JD015366, 2011.

Miyazaki, K., Eskes, H. J., and Sudo, K.: Global NOx emission estimates derived from an assimilation of OMI tropospheric NO2 columns, Atmos. Chem. Phys., 12, 2263–2288, https://doi.org/10.5194/acp-12-2263-2012, 2012.

Miyazaki, K., Sekiya, T., Fu, D., Bowman, K. W., Kulawik, S. S., Sudo, K., Walker, T., Kanaya, Y., Takigawa, M., Ogochi, K., Eskes, H., Boersma, K. F., Thompson, A. M., Gaubert, B., Barre, J., and Emmons, L. K.: Balance of Emission and Dynamical Controls on Ozone During the Korea-United States Air Quality Campaign From Multiconstituent Satellite Data Assimilation, J. Geophys. Res. Atmos., 124, 387–413, https://doi.org/10.1029/2018JD028912, 2019.

Miyoshi, T.: The Gaussian Approach to Adaptive Covariance Inflation and Its Implementation with the Local Ensemble Transform Kalman Filter, Mon. Weather Rev., 139, 1519–1535, https://doi.org/10.1175/2010MWR3570.1, 2011.

Miyoshi, T., Yamane, S., and Enomoto, T.: Localizing the Error Covariance by Physical Distances within a Local Ensemble Transform Kalman Filter (LETKF), SOLA, 3, 89–92, https://doi.org/10.2151/sola.2007-023, 2007.

Miyoshi, T., Sato, Y., and Kadowaki, T.: Ensemble Kalman Filter and 4D-Var Intercomparison with the Japanese Operational Global Analysis and Prediction System, Mon. Weather Rev., 138, 2846–2866, https://doi.org/10.1175/2010MWR3209.1, 2010.

Ott, E., Hunt, B. R., Szunyogh, I., Zimin, A. V., Kostelich, E. J., Corazza, M., Kalnay, E., Patil, D. J., and Yorke, J. A.: A Local Ensemble Kalman Filter for Atmospheric Data Assimilation, https://doi.org/https://doi.org/10.48550/arXiv.physics/0203058, 2002.

Ott, E., Hunt, B. R., Szunyogh, I., Zimin, A. V., Kostelich, E. J., Corazza, M., Kalnay, E., Patil, D. J., and Yorke, J. A.: A local ensemble Kalman filter for atmospheric data assimilation, Tellus A Dyn. Meteorol. Oceanogr., 56, 415–428, https://doi.org/10.3402/tellusa.v56i5.14462, 2004.

Patra, P. K., Niwa, Y., Schuck, T. J., Brenninkmeijer, C. A. M., Machida, T., Matsueda, H., and Sawa, Y.: Carbon balance of South Asia constrained by passenger aircraft CO2 measurements, Atmos. Chem. Phys., 11, 4163–4175, https://doi.org/10.5194/acp-11-4163-2011, 2011a.

Patra, P. K., Houweling, S., Krol, M., Bousquet, P., Belikov, D., Bergmann, D., Bian, H., Cameron-Smith, P., Chipperfield, M. P., Corbin, K., Fortems-Cheiney, A., Fraser, A., Gloor, E., Hess, P., Ito, A., Kawa, S. R., Law, R. M., Loh, Z., Maksyutov, S., Meng, L., Palmer, P. I., Prinn, R. G., Rigby, M., Saito, R., and Wilson, C.: TransCom model simulations of CH4 and related species: Linking transport, surface flux and chemical loss with CH4 variability in the troposphere and lower

stratosphere, Atmos. Chem. Phys., 11, 12813–12837, https://doi.org/10.5194/acp-11-12813-2011, 2011b.

Patra, P. K., Takigawa, M., Watanabe, S., Chandra, N., Ishijima, K., and Yamashita, Y.: Improved Chemical Tracer Simulation by MIROC4.0-based Atmospheric Chemistry-Transport Model (MIROC4-ACTM), SOLA, 14, 91–96, https://doi.org/10.2151/sola.2018-016, 2018.

Peters, W., Miller, J. B., Whitaker, J., Denning, A. S., Hirsch, A., Krol, M. C., Zupanski, D., Bruhwiler, L., and Tans, P. P.: An ensemble data assimilation system to estimate CO 2 surface fluxes from atmospheric trace gas observations, J. Geophys. Res., 110, D24304, https://doi.org/10.1029/2005JD006157, 2005.

Saunois, M., Stavert, A. R., Poulter, B., Bousquet, P., Canadell, J. G., Jackson, R. B., Raymond, P. A., Dlugokencky, E. J., Houweling, S., Patra, P. K., Ciais, P., Arora, V. K., Bastviken, D., Bergamaschi, P., Blake, D. R., Brailsford, G., Bruhwiler, L., Carlson, K. M., Carrol, M., Castaldi, S., Chandra, N., Crevoisier, C., Crill, P. M., Covey, K., Curry, C. L., Etiope, G., Frankenberg, C., Gedney, N., Hegglin, M. I., Höglund-Isaksson, L., Hugelius, G., Ishizawa, M., Ito, A., Janssens-Maenhout, G., Jensen, K. M., Joos, F., Kleinen, T., Krummel, P. B., Langenfelds, R. L., Laruelle, G. G., Liu, L., Machida, T., Maksyutov, S., McDonald, K. C., McNorton, J., Miller, P. A., Melton, J. R., Morino, I., Müller, J., Murguia-Flores, F., Naik, V., Niwa, Y., Noce, S., O'Doherty, S., Parker, R. J., Peng, C., Peng, S., Peters, G. P., Prigent, C., Prinn, R., Ramonet, M., Regnier, P., Riley, W. J., Rosentreter, J. A., Segers, A., Simpson, I. J., Shi, H., Smith, S. J., Steele, L. P., Thornton, B. F., Tian, H., Tohjima, Y., Tubiello, F. N., Tsuruta, A., Viovy, N., Voulgarakis, A., Weber, T. S., van Weele, M., van der Werf, G. R., Weiss, R. F., Worthy, D., Wunch, D., Yin, Y., Yoshida, Y., Zhang, W., Zhang, Z., Zhao, Y., Zheng, B., Zhu, Q., Zhu, Q., and Zhuang, Q.: The Global Methane Budget 2000–2017, Earth Syst. Sci. Data, 12, 1561–1623, https://doi.org/10.5194/essd-12-1561-2020, 2020.

Sekiya, T., Miyazaki, K., Ogochi, K., Sudo, K., Takigawa, M., Eskes, H., and Boersma, K. F.: Impacts of Horizontal Resolution on Global Data Assimilation of Satellite Measurements for Tropospheric Chemistry Analysis, J. Adv. Model. Earth Syst., 13, https://doi.org/10.1029/2020MS002180, 2021.

Skachko, S., Ménard, R., Errera, Q., Christophe, Y., and Chabrillat, S.: EnKF and 4D-Var data assimilation with chemical transport model BASCOE (version 05.06), Geosci. Model Dev., 9, 2893–2908, https://doi.org/10.5194/gmd-9-2893-2016, 2016.

Szopa, S., V. Naik, B. Adhikary, P. Artaxo, T. Berntsen, W.D. Collins, S. Fuzzi, L. Gallardo, A. Kiendler Scharr, Z. Klimont, H. Liao, N. U. and P. Zanis: Short-Lived Climate Forcers. In Climate Change 2021, Clim. Chang. 2021 Phys. Sci. Basis. Contrib. Work. Gr. I to Sixth Assess. Rep.

682 Intergov. Panel Clim. Chang., 2021.

683 Tian, X., Xie, Z., Liu, Y., Cai, Z., Fu, Y., Zhang, H., and Feng, L.: A joint data assimilation system
684 (Tan-Tracker) to simultaneously estimate surface CO2 fluxes and 3-D atmospheric CO2
685 concentrations from observations, Atmos. Chem. Phys., 14, 13281–13293,
686 https://doi.org/10.5194/acp-14-13281-2014, 2014.

687 Watanabe, S., Miura, H., Sekiguchi, M., Nagashima, T., Sudo, K., Emori, S., and Kawamiya, M.:
688 Development of an atmospheric general circulation model for integrated Earth system modeling on
689 the Earth Simulator, J. Earth Simulator, 9, 27–35, 2008.

690 van der Werf, G. R., Randerson, J. T., Giglio, L., van Leeuwen, T. T., Chen, Y., Rogers, B. M., Mu,
691 M., van Marle, M. J. E., Morton, D. C., Collatz, G. J., Yokelson, R. J., and Kasibhatla, P. S.: Global
692 fire emissions estimates during 1997–2016, Earth Syst. Sci. Data, 9, 697–720,
693 https://doi.org/10.5194/essd-9-697-2017, 2017.

694 Whitaker, J. S. and Hamill, T. M.: Evaluating Methods to Account for System Errors in Ensemble
695 Data Assimilation, Mon. Weather Rev., 140, 3078–3089, https://doi.org/10.1175/MWR-D-11-
696 00276.1, 2012.

697 Yoshida, Y., Kikuchi, N., Morino, I., Uchino, O., Oshchepkov, S., Bril, A., Saeki, T., Schutgens, N.,
698 Toon, G. C., Wunch, D., Roehl, C. M., Wennberg, P. O., Griffith, D. W. T., Deutscher, N. M.,
699 Warneke, T., Notholt, J., Robinson, J., Sherlock, V., Connor, B., Rettinger, M., Sussmann, R.,
700 Ahonen, P., Heikkinen, P., Kyrö, E., Mendonca, J., Strong, K., Hase, F., Dohe, S., and Yokota, T.:
701 Improvement of the retrieval algorithm for GOSAT SWIR XCO 2 and XCH 4 and their validation
702 using TCCON data, Atmos. Meas. Tech., 6, 1533–1547, https://doi.org/10.5194/amt-6-1533-2013,
703 2013.

704 Zhang, F., Snyder, C., and Sun, J.: Impacts of Initial Estimate and Observation Availability on
705 Convective-Scale Data Assimilation with an Ensemble Kalman Filter, Mon. Weather Rev., 132,
706 1238–1253, https://doi.org/10.1175/1520-0493(2004)132<1238:IOIEAO>2.0.CO;2, 2004.

707 Zhang, Y., Jacob, D. J., Lu, X., Maasakkers, J. D., Scarpelli, T. R., Sheng, J.-X., Shen, L., Qu, Z.,
708 Sulprizio, M. P., Chang, J., Bloom, A. A., Ma, S., Worden, J., Parker, R. J., and Boesch, H.:
709 Attribution of the accelerating increase in atmospheric methane during 2010–2018 by inverse analysis
710 of GOSAT observations, Atmos. Chem. Phys., 21, 3643–3666, https://doi.org/10.5194/acp-21-3643-
711 2021, 2021.

712